

Coalescence of magnetic islands including anomalous resistivity

J. Schumacher and B. Kliem

Astrophysical Institute Potsdam, An der Sternwarte 16, D-14482 Potsdam, Germany

(Received 10 March 1997; accepted 30 June 1997)

Two-dimensional compressible magnetohydrodynamic simulations of the coalescence instability in a low-beta plasma are presented in which anomalous resistivity is permitted to occur. The instability is considered in a uniform current sheet configuration, initially perturbed by an infinite chain of spots of anomalous resistivity. The two phases of the instability known from simulations based on the Fadeev equilibrium—ideal and resistive—can clearly be distinguished also in this configuration. It is found that the conversion of magnetic energy into kinetic energy dominates Ohmic heating. The main energy release occurs within a few Alfvén transit times. The scaling of several key parameters in the current layer formed between the coalescing islands is compared to the scalings obtained with uniform resistivity. The numerical results indicate that the peak reconnection rate decreases toward large Lundquist numbers ($S \gg 10^4$) as $S^{-\alpha}$ with $\alpha = \frac{1}{5} - \frac{1}{3}$ and that a transition to slow reconnection ($\alpha \sim \frac{1}{2}$) may occur at $S \gtrsim 10^7$, where S is based on the background resistivity. © 1997 American Institute of Physics. [S1070-664X(97)01110-5]

I. INTRODUCTION

The dynamics of current sheets is an important key for the understanding of eruptive energy releases in astrophysical and laboratory plasmas. The stored magnetic energy can be converted by a variety of magnetohydrodynamic (MHD) and kinetic plasma instabilities, e.g., the tearing instability, the coalescence instability, current-driven kinetic instabilities, and the radiative instability. The coalescence instability of magnetic islands, or current filaments, an ideal MHD instability, is of particular interest for at least two reasons. First, it develops more rapidly and releases more energy than the tearing instability and, second, it involves the formation of a new current sheet between the approaching islands, where magnetic reconnection can be studied free of boundary conditions with prescribed inflow. The instability has been studied analytically by Finn and Kaw¹ and numerically in a series of MHD and particle simulations. Its nonlinear development was first investigated by Pritchett and Wu,² who numerically determined the growth rate as a function of the Lundquist number, $S = \mu_0 L V_A / \eta_0$, and found strong pileups of the current density between the coalescing islands. Biskamp and Welter³ (BW) divided the development of the coalescence into an ideal phase, during which the magnetic islands approach each other as a whole, and a resistive phase, during which reconnection of magnetic field lines between the attracting islands permits completion of the instability. They empirically deduced scaling laws for varying Lundquist number of certain key parameters of the newly formed current sheet between the coalescing islands in the incompressible case. These parameters include its half-width δ , its length Δ , and the upstream magnetic field B_y . Their scaling laws predict high reconnection rates, $R \sim S^0$, exceeding those of Petschek-type reconnection, for relatively large values of S ($\sim 10^3 - 10^4$). At much higher values of S , however, BW expect much lower reconnection rates of the order of the Sweet–Parker scaling, $R_{SP} \sim S^{-1/2}$, unless anomalous resistivity occurs, which is, in fact, expected due to their rapidly decreasing current layer width, $\delta \sim S^{-2/3}$. Bhattacharjee

*et al.*⁴ found indications for a transition from Sweet–Parker-type to Petschek-type reconnection rates at this current sheet for more strongly peaked initial current density profiles and increasing compressibility of the plasma. Rickard and Craig⁵ (RC), using moderately peaked initial current density profiles similar to Biskamp and Welter, also found a rise of the reconnection rate with the inclusion of compressibility, but scalings with the Lundquist number identical to Biskamp and Welter. Tajima *et al.*⁶ compared particle and MHD simulations of coalescence. They observed an explosive energy release during the coalescence and subsequent oscillations of kinetic energy by both methods. Scholer⁷ found that the energy release during coalescence of islands exceeds the energy release during island formation by tearing (similar to Leboeuf *et al.*⁸) and that there is little influence of the Lundquist number on the amount of released energy (in a range of relatively small Lundquist numbers). On the other hand, Matthaeus and Lamkin⁹ obtained higher kinetic energies for higher S in a similar system, where turbulent fluctuations were amplified by the evolving coalescence instability.

Most of these investigations^{1-6,8} used the Fadeev equilibrium,¹⁰ a generalization of the Harris current sheet equilibrium containing an infinite chain of magnetic islands with current density maxima located at the O points, a velocity perturbation to initiate coalescence, and constant resistivity η_0 . The Fadeev equilibrium contains a free parameter (ϵ in the notation of Pritchett and Wu) describing the peakedness of the current density profile; the majority of results in the literature was obtained for $\epsilon = 0.2 - 0.3$. An alternative approach, which appears more natural for space and astrophysical plasmas, uses a tearing mode instability in a uniform current sheet to create the island chain and an appropriate small additional perturbation to initiate coalescence, which may be broadband noise^{7,9} or a weak tearing mode of double wavelength.¹¹ Although the current density peaks at the X points in this case, coalescence occurs also, together with acceleration of the islands as a whole and a correspondingly rapid rise of the kinetic energy.

In the present paper a third dynamical path to coalescence is considered. It is supposed that the excitation of anomalous resistivity at several locations in an extended uniform current sheet creates the island chain and initiates the coalescence. This is particularly relevant for plasmas at high Lundquist numbers, where tearing mode growth rates are small and spontaneous tearing can easily be suppressed, e.g., by flows.¹² Then, a current sheet driven by external motions¹³ or formed through the loss of equilibrium¹⁴ shrinks to a width where effects not contained in classical MHD become important. As discussed below, for low plasma beta ($\beta \ll 1$) a kinetic current-driven instability giving rise to localized anomalous resistivity is the first relevant effect. Anomalous resistivity is permitted to occur also at later times in the evolution of the coalescence instability, which takes into account the high current density pileup that occurs between the coalescing islands for high values of the Lundquist number.^{2,3} If a current sheet is perturbed by a finite or irregular chain of anomalous resistivity spots, a complex sequence of island formation and dynamics occurs, including tearing, coalescence, and acceleration and the ejection of islands.¹⁵ Here we consider an infinite regular chain of anomalous resistivity spots in a simulation box with periodic boundaries along the current sheet, in order to concentrate on the coalescence instability. As a further difference to most of the previous coalescence simulations, natural for astrophysical plasmas, open boundaries are used in the perpendicular direction. Only Richard *et al.*¹⁶ have previously discussed the coalescence in current sheets with open boundaries (in the x and y directions), observing higher flow velocities and correspondingly higher kinetic energy increase than in systems with closed or periodic boundaries.

Which kinetic instability has the lowest threshold depends on the current sheet structure and the plasma parameters. The lower-hybrid-drift (LHD) instability, the ion acoustic instability, and the ion cyclotron instability appear to be the most important ones.¹⁷ For small and intermediate values of the plasma beta, the LHD instability has the lowest threshold,¹⁸ $j_{\text{cr}} \lesssim nev_{ti}$ for $\beta \lesssim 1$, where $v_{ti} = (T_i/m_i)^{1/2}$. Accordingly, it has been considered as the primary candidate for triggering substorm energy release in the geomagnetic tail.^{19,20} Increasing β suppresses the instability, the critical β value depending on T_e/T_i and j/nev_{ti} , being of order $\beta \sim 1-5$ in a relatively broad range of these parameters.^{21,20} Also, increasing magnetic shear reduces the LHD growth rate but the instability appears to be robust against a considerable amount of shear if the density gradient scale is much smaller than the ion cyclotron radius, which is the case for $\beta \ll 1$.²² If the LHD instability is suppressed, then the ion acoustic instability is relevant in the range $T_e \gtrsim 10T_i$ with a threshold²³ $j_{\text{cr}} \gtrsim 4nev_{ti}$. For $T_e \lesssim 10T_i$ the ion cyclotron instability will occur; its threshold is²⁴ $j_{\text{cr}} \approx 12(T_i/T_e)nev_{ti}$.

The critical current density corresponds to a critical current sheet half-width $l_{\text{cr}} = B/\mu_0 j_{\text{cr}}$. This has to be compared to the characteristic scales of those terms that are usually considered small in generalized Ohm's law. These scales are $L_H \sim \delta_i = c/\omega_{pi}$, $L_p \sim (\beta/4)\delta_i$, and $L_{in} \sim \delta_e = c/\omega_{pe}$ for the Hall, pressure gradient, and inertial terms, respectively. The inertial term must be compared with the resistive term

ηj , since, in general, these two support a parallel electric field. Their ratio is $(\delta_e/l_{\text{cr}})^2 S_{\text{an}}$. Here the Lundquist number S_{an} is based on the anomalous resistivity η_{an} . Using $j_{\text{cr}} = nev_{ti}$ (and $T_e = T_i$ for simplicity), we find $l_{\text{cr}} = 4\beta^{-1}r_{ci}$, where r_{ci} is the ion cyclotron radius, and $(\delta_e/l_{\text{cr}})^2 = (m_e/4m_i)\beta$. Let us use the anomalous resistivity produced by the LHD instability,¹⁷ $\eta_{\text{anLHD}} = 2\pi\omega_{\text{LH}}/\omega_{pe}^2 = (v_{ti}/c) \times (\Lambda/\ln \Lambda)\beta^{-1/2}\eta_0$, in estimating the ratio of the inertial and resistive terms. Here ω_{LH} is the lower hybrid frequency, Λ is the number of particles per Debye sphere, and η_0 is the background resistivity. It is seen that in hot but nonrelativistic plasmas $\eta_{\text{an}}/\eta_0 \sim 10^4-10^5$ so that the inertial term remains small for $S \lesssim 10^8$ and $\beta \lesssim 1$. A similar result is obtained for the ion acoustic instability (using $\eta_{\text{an}}/\eta_0 \sim 10^{-2}\omega_{pe}/\nu_{\text{coll}}$). The ratio of the Hall and pressure gradient terms to the convective term in Ohm's law at the threshold of kinetic instability is, respectively, δ_i/l_{cr} and $(\beta/4)\delta_i/l_{\text{cr}}$. Using again $l_{\text{cr}} = 4\beta^{-1}r_{ci}$, we see that $\delta_i/l_{\text{cr}} = \beta^{1/2}/2$ and that both terms remain small at the threshold of kinetic instability for $\beta \ll 1$. We confirm *a posteriori* using the simulation results that the diffusion region built up by anomalous resistivity, although being pushed to scales smaller than l_{cr} during the most dynamical phases of coalescence, remains sufficiently broad to keep the Hall and pressure gradient terms smaller than the convective term over most of the region for $\beta \ll 1$ (Sec. III C 3). For $\beta \gtrsim 1$ the ion and the electron fluid motions decouple ($l_{\text{cr}} \lesssim \delta_i$) and both terms should be retained in the description that is then based on electron magnetohydrodynamics and its generalizations. In these equations the Hall term introduces the dispersive whistler mode that permits high reconnection rates in spite of low resistivity.^{25,26} Using parameters of the lower solar corona prior to flares for illustration ($B_0 = 200$ G, $n_0 = 10^{10}$ cm⁻³, $T_0 = 2.5 \times 10^6$ K), we find $S(L=l_{\text{cr}}) = 7 \times 10^8$ and $\beta = 4 \times 10^{-3}$.

In the following we study the dynamical evolution of the coalescence instability under the action of anomalous resistivity in two-dimensional, compressible current sheets. The evolution turns out to be similar in several basic properties to the cases investigated previously. The conversion of magnetic energy into kinetic energy and heat will be studied in detail. We examine the scaling laws of several quantities with the Lundquist number, such as the maximum current densities and maximum reconnection rates of the whole simulation domain. Further, the key quantities of the current layer formed between the coalescing islands are considered for varying S . We compare these scaling laws with their counterparts from simulations with constant resistivity in order to see whether high reconnection rates at large S occur here, too.

II. SIMULATION MODEL

The compressible plasma is modeled by the following equations:

$$\partial_t \rho + \nabla \cdot (\rho \mathbf{u}) = 0, \quad (1)$$

$$\rho \partial_t \mathbf{u} + \rho (\mathbf{u} \cdot \nabla) \mathbf{u} = -\nabla p + \mathbf{j} \times \mathbf{B}, \quad (2)$$

$$\partial_t \mathbf{B} = \nabla \times (\mathbf{u} \times \mathbf{B}) - \nabla \times (\eta \mathbf{j}), \quad (3)$$

$$\partial_t U + \nabla \cdot \mathbf{S} = 0, \quad (4)$$

where the current density \mathbf{j} , the total energy density U , and the flux vector \mathbf{S} are given by

$$\mathbf{j} = \frac{1}{\mu_0} \nabla \times \mathbf{B},$$

$$U = \rho e + \frac{\rho}{2} u^2 + \frac{B^2}{2\mu_0},$$

$$\mathbf{S} = \left(U + p + \frac{B^2}{2\mu_0} \right) \mathbf{u} - (\mathbf{u} \cdot \mathbf{B}) \frac{\mathbf{B}}{\mu_0} + \eta \mathbf{j} \times \frac{\mathbf{B}}{\mu_0},$$

and e is the internal energy per unit mass, which is related to the pressure through the equation of state, $p = (\gamma - 1)\rho e$. In the two-dimensional model adopted here, $\partial/\partial z = 0$ for all quantities and $B_z = u_z = 0$; hence the current density and the electric field possess only z components; further, the ratio of specific heats $\gamma = 2$. The electric field is given by $\mathbf{E} = -\mathbf{u} \times \mathbf{B} + \eta \mathbf{j}$.

A two-step Lax–Wendroff scheme with artificial smoothing and an adaptive time step is used.^{27,15} The variables are normalized in the conventional manner²⁷ by quantities derived from the current sheet half-width l_{CS} and the asymptotic ($y \rightarrow \infty$) Alfvén velocity $V_{A0} = B_0 / (\mu_0 \rho_0)^{1/2}$ of the configuration at $t = 0$. Thus the background resistivity is given by $\eta_0 = S^{-1}$. Henceforth we use only normalized quantities. The box dimensions are $L_x = 21$ and $L_y = 3$. A high spatial resolution is taken with $\Delta x = \Delta y = \frac{1}{48}$ up to $\Delta x = \Delta y = \frac{1}{70}$. The following magnetostatic equilibrium with uniform density is chosen as the initial condition:

$$B_x = \begin{cases} -\sin(\pi y/2): & 0 \leq y \leq 1, \\ -1: & y > 1, \end{cases}$$

$$B_y = u_x = u_y = 0,$$

$$\rho = 1,$$

$$p = 1 + \beta - B^2(y),$$

where the plasma beta is defined as $\beta = 2\mu_0 p(|y| \rightarrow \infty) / B_0^2$. The plasma beta is $\beta = 0.1$ for all runs presented in Sec. III so that compressibility effects can be expected to play a role (comparison runs with $\beta = 10^{-3} - 1$ are discussed in Sec. III C 3).

Symmetrical boundary conditions are chosen at the lower boundary ($y = 0$). At $y = L_y$ open boundary conditions are realized by the requirement that the normal derivative of all variables vanishes, except for the normal component of \mathbf{B} , which is determined from the solenoidal condition. Periodic boundary conditions are used in the x direction.

The magnetostatic equilibrium is initially perturbed by an anomalous resistivity profile. Two spots of enhanced resistivity are introduced into the simulation domain for $0 \leq t \leq t_0$ (with $t_0 = 4$ in all cases presented):

$$\eta(x, y, t \leq t_0) = \max \left(\eta_0; \sum_{i=1}^2 A_i \exp[-(r_i/r_0)^3] \right),$$

where r_i is the distance to the i th spot at position $(x_i, 0)$. The positions of the resistivity maxima are $x_1 = 0$ ($= L_x$ due to

periodicity in x) and $x_2 = L_x/2$. The parameter r_0 , taken to be unity, characterizes the width of the spots, and the A_i denote their amplitudes, which were set to $A_1 = 0.03$ and $A_2 = 0.02$ in the majority of runs. Choosing unequal amplitudes leads to both island formation and island coalescence without further perturbations. Some scatter of the amplitudes can be expected in natural systems due to variation of the plasma parameters along the current sheet. For $t > t_0$ the resistivity is determined self-consistently from the local value of the current density for every time step: an ‘‘anomalous’’ value η_{an} is set if a threshold, j_{cr} , is exceeded. Employing two different models of the anomalous resistivity, we confirm the expectation that the dynamic evolution and the scaling of the reconnection rate do not sensitively depend on the particular choice of that model. The first, linear, model is given by

$$\eta_1(x, y, t > t_0) = \begin{cases} \eta_0: & |j| \leq j_{cr}, \\ C\eta_0(|j| - j_{cr}) + \eta_0: & |j| > j_{cr}. \end{cases} \quad (5)$$

The second model uses a quadratic dependence of the anomalous resistivity on the local current density overshoot:

$$\eta_2(x, y, t > t_0) = \begin{cases} \eta_0: & |j| \leq j_{cr}, \\ C\eta_0(|j| - j_{cr})^2 + \eta_0: & |j| > j_{cr}, \end{cases} \quad (6)$$

where $j_{cr} = 2 = (4/\pi)j(x, 0, 0)$ and $C = 10$ for all runs and both models. The parameter C is chosen such that the anomalous resistivity rises rapidly once the threshold is exceeded, while retaining numerical stability over a broad range of Lundquist numbers. A linear dependence of the anomalous resistivity on the current density is expected in case of the ion acoustic instability and a quadratic dependence is expected in case of the lower-hybrid-drift instability.¹⁷

III. RESULTS OF THE SIMULATIONS

A. Time development

A detailed description of the dynamic evolution is given for the representative case $S = 1000$, $A_1/A_2 = 1.5$, and the linear anomalous resistivity model. The evolution turns out to be nearly identical for the quadratic η_{an} model. Figure 1 shows a time sequence of the magnetic field and the velocity field. The initial perturbation causes a chain of magnetic islands, which we refer to as ‘‘induced tearing.’’ The typical flow pattern known from simulations with a single resistivity spot²⁷ develops in this period: the Lorentz force leads to outflows in the x direction from the η_{an} spots, which drags inflows in the y direction into these areas. This is connected with a recovery of the current density for $t > t_0$; a short current sheet-like structure with current density maxima at the X points develops subsequently. At $t \approx 10$ anomalous resistivity is switched on at both X points, which tends to stabilize the reconnection flow pattern at the X points.²⁷ However, the flow gradually changes to a near-uniform bulk flow of the whole island toward the inner, weaker X point, characteristic of the coalescence instability,^{2-8,11,15,16} and reverses the original reconnection flow at the inner X point [see $t = 41$ in Fig. 1(b)].

The phase of island approach starts right after the initial perturbation, as is evident from Fig. 2, which shows the po-

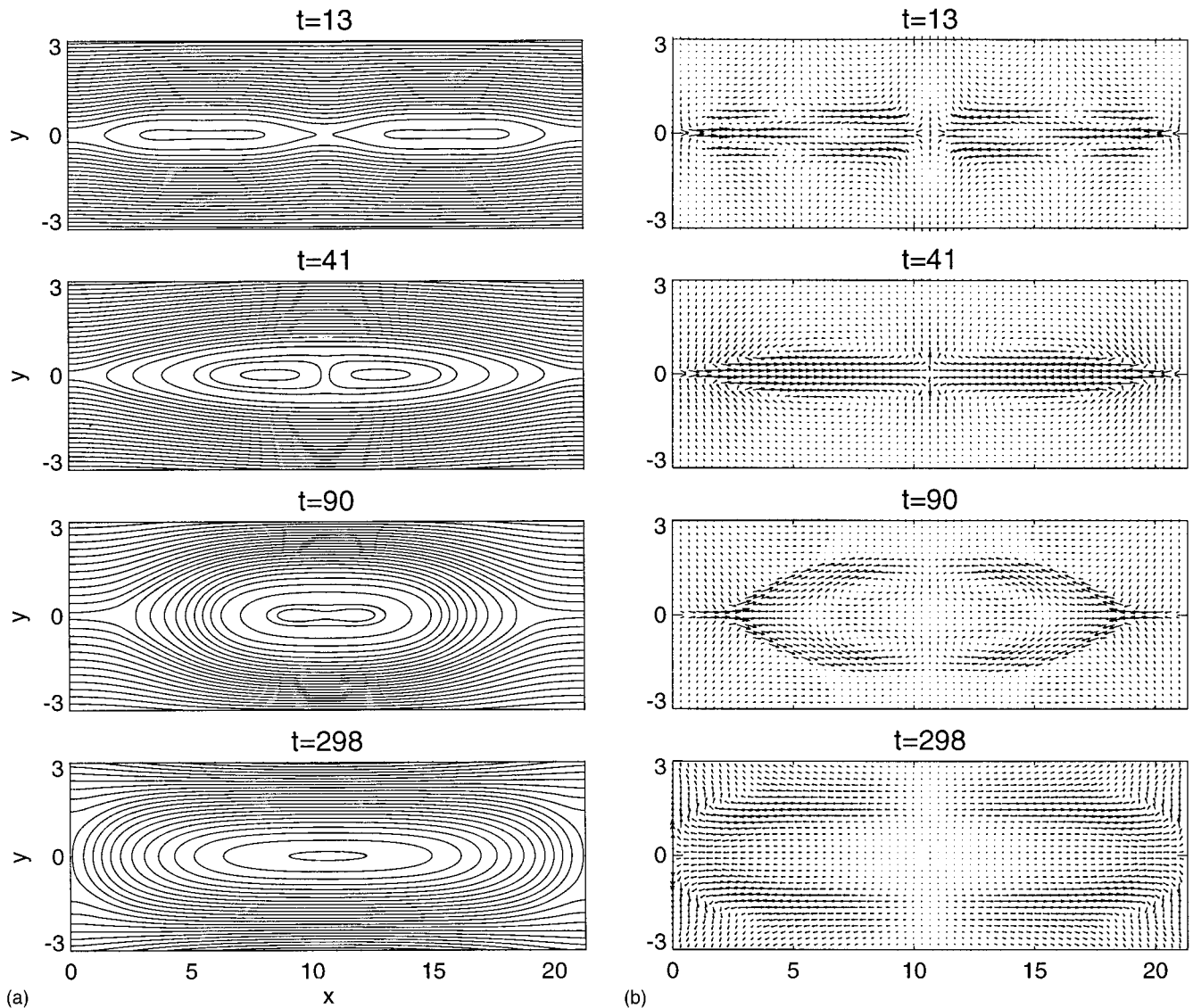


FIG. 1. Development of the coalescence instability for $S = 1000$, $\beta = 0.1$, and $j_{cr} = 2$ using the linear resistivity model. (a) Magnetic field lines. (b) Velocity field. Maximum velocities are, in order of increasing time, 0.16, 0.36, 0.6, and 0.21.

sition of the O points as a function of time. A displacement of the O points with a nearly constant velocity of 0.16 is observed in this first phase of coalescence ($t \approx 4-35$). The O-point velocity is independent of the Lundquist number over the full range of values studied here, hence, this phase represents an ideal phase of the coalescence instability. We remind that the initial anomalous resistivity perturbation ($t < t_0$) does not depend on S , while the anomalous resistivity occurring later [Eqs. (5) and (6)] is proportional to S^{-1} . This suggests that the difference between the fluxes reconnected at the stronger and the weaker X point, respectively, i.e., the existence of field lines enclosing both islands, is the main driver of the approach, since it is created by the initial perturbation to a large extent. On the other hand, the acceleration of the jet-like outflows from the stronger X point by the Lorentz force jB_y , which also drives the coalescence, does depend on S , as evident from Table I, where the peak values of these outflows are listed. Their contribution to the bulk flow leads to small differences in the O-point velocity seen

in Fig. 2 in the interval $t \approx 35-50$, in which a transition between the ideal phase and the resistive phase takes place.

The island approach is connected with the slow destruction of the current density enhancement at $x = L_x/2$ during $t \approx 15-30$. For $t > 30$ a pileup to negative values of j develops at $x = L_x/2$, reaching a minimum of $j(L_x/2, 0) = -2.1$ at $t = 41$ (as seen in the lower panel of Fig. 2). The structure of the newly formed current layer is shown in Fig. 3, where the magnetic field, the velocity field, the current density, and the anomalous resistivity are plotted around $(L_x/2, 0)$ at $t = 41$. The plasma is streaming toward this sheet and is decelerated, accompanied by a strong pileup of B_y . It is ejected in the y direction with $u_y \approx 0.13$. Anomalous resistivity is excited in a thin region around the current density minimum. The quadratic η_{an} model leads to an identical shape of this current layer.

The coalescence is driven to completion and the central current layer is slowly destroyed in the time period $t = 57-140$. This second, resistive, phase is accompanied by

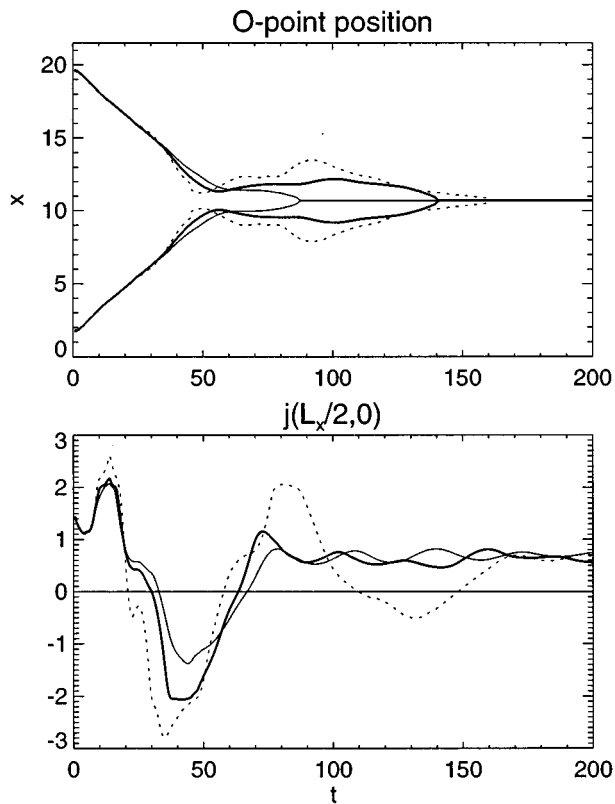


FIG. 2. Position of the O points in the upper panel and the current density j at $(L_x/2,0)$ in the lower panel versus time for the simulations with $S=750$ (thin solid line), $S=1000$ (thick solid line), and $S=2500$ (dashed line) and the linear resistivity model.

oscillations of the newly formed island with periods of several tens of Alfvén times. Such oscillations have also been observed in previous simulations that had taken the Fadeev equilibrium as the initial condition. Strong jets from the outer X point with maximum velocities $u_{x,max}=0.8$ support the coalescence in this phase and form a plasmoid (i.e., a high-pressure region) by pumping plasma into the island. The resistive phase of completion of island merging slows down with increasing Lundquist number, as is visible in the upper panel of Fig. 2. The reconnection outflows from the outer X point decay with the growing size of the plasmoid, and the expanding plasmoid eventually fills the whole box.

TABLE I. Maximum ratios of the global energy conversion rates and of the time-averaged global energy conversion rates, and the global maximum of u_x (taken from t_0 to the time at which maximum flux pileup between the coalescing islands is observed) for the linear anomalous resistivity model, Eq. (5).

S	$\max[W_1(t)/\epsilon_m(t)]$	$\max[\langle W_1 \rangle_t / \langle \epsilon_m \rangle_t]$	$\max[u_x]$
500	0.5	<1.0	0.2
750	4.2	2.0	0.3
1000	7.2	2.2	0.4
1500	6.8	2.7	0.6
2500	7.3	2.7	0.8
5000	7.0	2.8	0.8
10 000	7.3	3.1	0.9

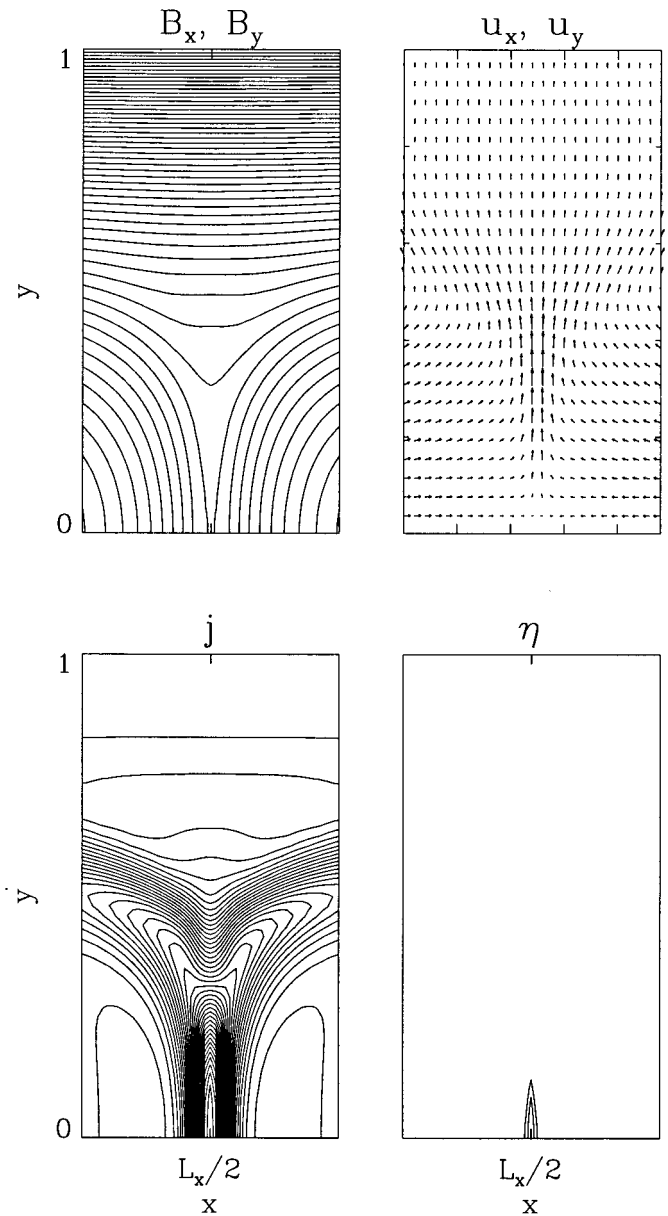


FIG. 3. Detailed structure of the magnetic field, velocity field, current density, and anomalous resistivity at the time of maximum current density pileup between the coalescing islands ($t=41$) for the simulation shown in Fig. 1.

Varying the ratio of the initial η_{an} amplitudes by choosing $A_2=0.015$ and $A_2=0.025$ (with $S=1000$) does not qualitatively change the evolution of the instability. The main effect consists of a stretching of the ideal phase of the island approach with decreasing A_1/A_2 since the flow around the weaker X point then resists the coalescence flow over a longer period. The energy conversion rates and the peak reconnection rates discussed below are only weakly affected. All subsequent results are given for $A_2=0.02$.

Also, the influence of the upper boundary condition on the results was found to be weak by comparing two runs with open (closed) boundary at $L_y=3$ (5) and otherwise identical setup (at $S=2500$). The current density maxima and minima occurred at the same time and differed by less than 4%.

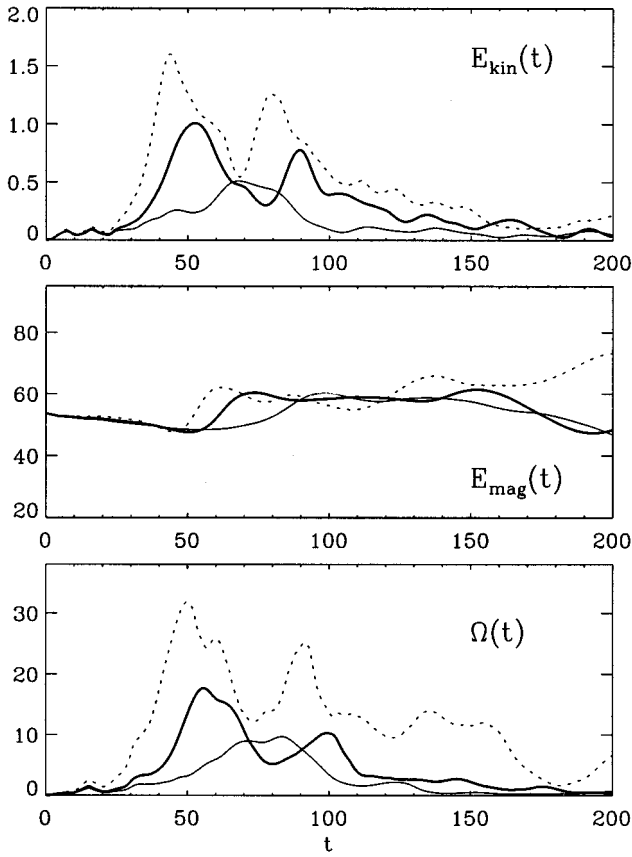


FIG. 4. Development of the kinetic energy, magnetic energy, and enstrophy in the simulations with $S=750$ (thin solid line), $S=1000$ (thick solid line), and $S=2500$ (dashed line) using the linear resistivity model.

B. Energy conversion

The time histories of the magnetic energy $E_{\text{mag}} = \int_F B^2 dF$, the kinetic energy $E_{\text{kin}} = \int_F \rho u^2 dF$, and the enstrophy $\Omega = \int_F |\nabla \times \mathbf{u}|^2 dF$, where F denotes the whole simulation domain, are shown in Fig. 4 for $S=750$, 1000, 2500, and the η_1 model. Two peaks in the kinetic energy are clearly visible. The first one corresponds to the development of the typical bulk flow pattern of coalescence during its ideal phase. The second peak is caused by the strong plasma jets from the outer X point. The magnetic energy is continuously decreasing for the first 50 Alfvén times. The coalescence instability transforms a certain amount of the stored magnetic energy into kinetic energy. At later times, the magnetic energy density in the box is increasing again, due to inflows driven by the dominant X point.

The enstrophy $\Omega(t)$, a measure of the strength of the vorticity in the fluid, behaves very similarly to the kinetic energy. The development of coherent large vortex structures leads to an increase of the vorticity. The bulk flow pattern with the return flows in the first coalescence phase [$t=41$ in Fig. 1(b)] represents such a structure and gives the main contribution to $\Omega(t)$. It is found that the maxima of E_{kin} and Ω increase with increasing S . Scholer⁷ observed the same behavior for Ω in his simulations by comparing the enstrophy for runs with $S=118$ and $S=294$, but did not obtain a corresponding increase of E_{kin} . This difference is due to the

jet acceleration by the outer X point in our calculations, which does depend on S . The growth time up to $\max(E_{\text{kin}})$ and $\max(\Omega)$ decreases with increasing S , i.e., the energy conversion becomes more rapid for higher Lundquist numbers.

Let us now study the conversion of magnetic energy in more detail and quantitatively by considering the electromagnetic energy balance, given in dimensionless form by

$$\partial_t B^2 = -2\eta j^2 - 2\mathbf{u} \cdot (\mathbf{j} \times \mathbf{B}) - 2\nabla \cdot (\mathbf{E} \times \mathbf{B}). \quad (7)$$

The first term on the right-hand side of Eq. (7) gives the conversion of magnetic into thermal energy by Ohmic dissipation. The second term measures that part of the magnetic energy that is directly exchanged with the kinetic energy. If it is positive, the Lorentz force density $\mathbf{f}_L = \mathbf{j} \times \mathbf{B}$ transfers energy to the fluid. We consider two measures of the *global* energy conversion, the dissipation rate, and the conversion rate of magnetic into kinetic energy, integrated over the simulation domain F , and given by, respectively,

$$\epsilon_m(t) = \int_F \eta j^2 dF,$$

$$W_L(t) = \int_F \mathbf{u} \cdot (\mathbf{j} \times \mathbf{B}) dF.$$

It is also of interest to compare the following averages:

$$\langle \epsilon_m \rangle_t = \frac{1}{t-t_0} \int_{t_0}^t \epsilon_m(\tau) d\tau,$$

$$\langle W_L \rangle_t = \frac{1}{t-t_0} \int_{t_0}^t W_L(\tau) d\tau.$$

They denote the mean conversion rates evaluated from t_0 , the time when the initial perturbation is switched off, up to a time t of the dynamic development. Their ratio indicates which energy conversion process dominates up to this time. These four functions are shown in Fig. 5 for the run with $S=1000$. It is seen that while conversion into kinetic energy dominates over large parts of the evolution, Ohmic heating is nearly equally important if the coalescence process is considered as a whole. The maximum ratio of both time averages is given in Table I; it is slowly increasing with increasing Lundquist number. For comparison, the maximum ratio of the two conversion rates is also listed. The nearly uniform acceleration of the islands as a whole is apparent in the rise of $\langle W_L \rangle_t$ by nearly two orders of magnitude during $t=20-60$, i.e., during only ≈ 4 Alfvén transit times based on the initial O-point separation. The function $W_L(t)$ best reflects the oscillations of the flow during coalescence, discussed above. The figure shows that the energy conversion is nearly independent of the choice of the anomalous resistivity model.

The coalescence instability provides a period of dynamic current sheet development during which the conversion of E_{mag} into E_{kin} dominates in comparison to Ohmic dissipation. Table I shows that this is the case for Lundquist numbers $S \geq 750$. The main contribution to the Ohmic dissipation comes from the anomalous resistivity area at the outer X point.

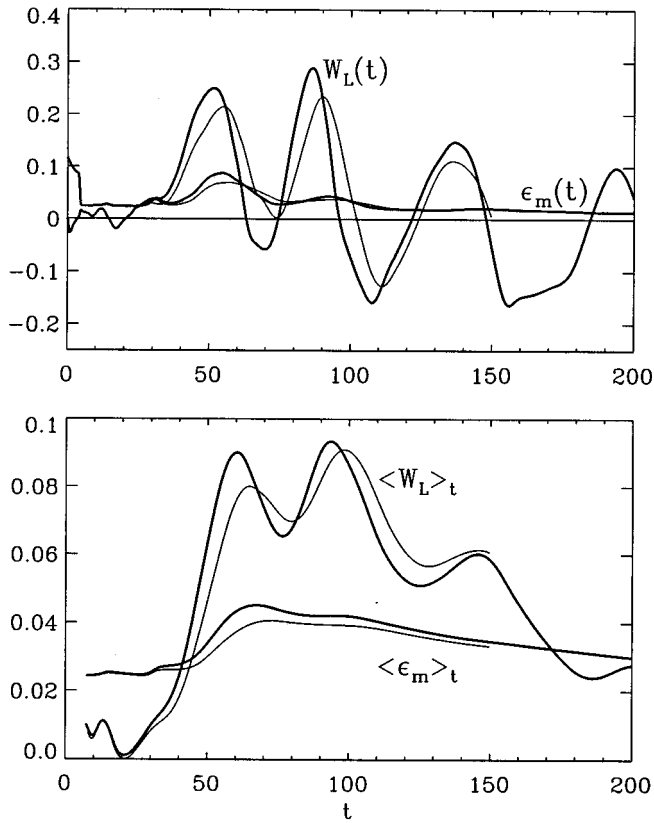


FIG. 5. Conversion rate between the magnetic and kinetic energy, $W_L(t)$, and Ohmic heating rate, $\epsilon_m(t)$ (upper panel), and the corresponding time-averaged conversion rates (lower panel) for $S=1000$. Thick lines correspond to the linear η_{an} model [Eq. (5)]; thin lines correspond to the quadratic η_{an} model [Eq. (6)].

C. Scaling laws

1. Linear anomalous resistivity model

First we are interested in the scaling of the maximum current density j and the maximum reconnection rate R_1^o

$= \max[\eta_l j(0,0)]$, which occur at the driving outer X point, with the Lundquist number. In this and subsequent scalings, the Lundquist number refers to the background resistivity, $S = \mu_0 I_{CS}(t=0) V_{A0} / \eta_0$. Only the interval $t_0 < t < t_{\min}$ is considered, where t_{\min} is the time at which the current density between the coalescing islands becomes minimal (cf. Fig. 2). As Fig. 6 shows, the following power law fits the numerical results for the maximum current density very well:

$$j = 0.27 S^{0.35}. \quad (8)$$

The system develops higher current density overshoots over j_{cr} for increasing Lundquist number. Inserting (8) into (5), the reconnection rate becomes

$$R_1^o = 0.73 S^{-0.3} - 5.1 S^{-0.65}. \quad (9)$$

Although smaller than the Petschek reconnection rate²⁸ $R_p = \pi / (8 \ln S)$, the rate R_1^o exceeds the Sweet–Parker rate $R_{SP} = S^{-1/2}$ in the range of astrophysical interest and may in this sense be regarded as “fast.”

We now turn to the consideration of the dynamics in the inner current sheet between the coalescing islands. We expect scaling laws at this current sheet not to be independent of the scaling laws at the outer X point, or outer current sheet, since the latter is an active element in the system (in contrast to constant resistivity simulations) and is dynamically coupled to the inner current sheet by the flow. Quantities to examine are the current sheet half-width δ , the current sheet length Δ , the current density minimum at the coalescence point $j(L_x/2, 0)$, the reconnection rate $R_1^i = |\min[\eta_l j(L_x/2, 0)]|$, the maximum magnetic field B_y at this current sheet, the inflow speed u_x , and the maximum outflow speed u_y . The current sheet half-width is determined by fitting the current density profile with a $\cosh^{-2}(x/\delta)$ function, and the inflow speed is taken at the point of maximum B_y . All values are determined at $t = t_{\min}$. Thus, in the following we discuss the peak reconnection rates during coalescence,

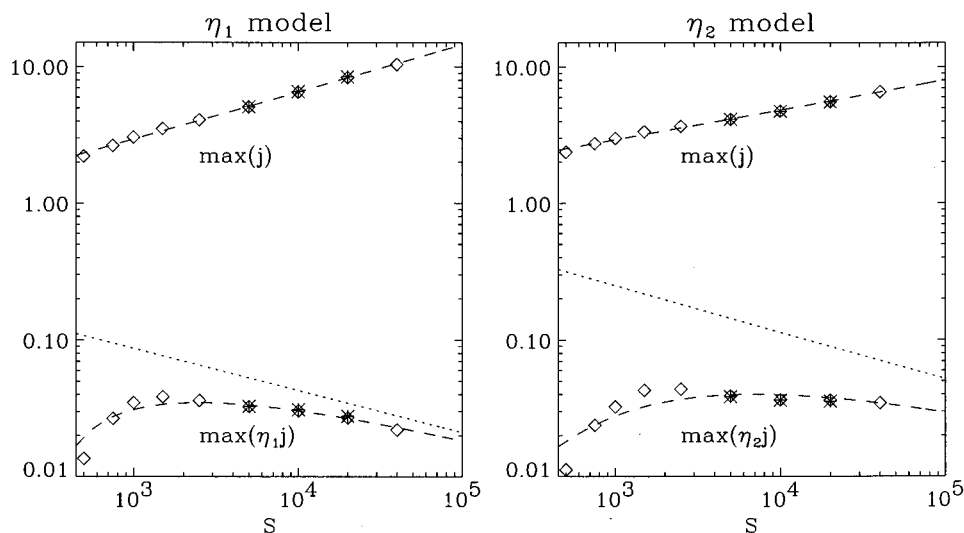


FIG. 6. Dependence of the maximum current density and the maximum reconnection rate at the outer X point on the Lundquist number for both resistivity models. Left panel: $\eta = \eta_1$; dashed lines show the fits according to Eqs. (8) and (9), and the dotted line is the asymptotic scaling, $R_1^o \sim S^{-0.3}$. Right panel: $\eta = \eta_2$; dashed lines are the fit results given in Eqs. (17) and (18), and the dotted line is the asymptotic scaling $R_2^o \sim S^{-0.34}$. Diamonds represent simulations with $\Delta x = \Delta y = \frac{1}{48}$; asterisks show comparison runs with $\Delta x = \Delta y = \frac{1}{70}$.

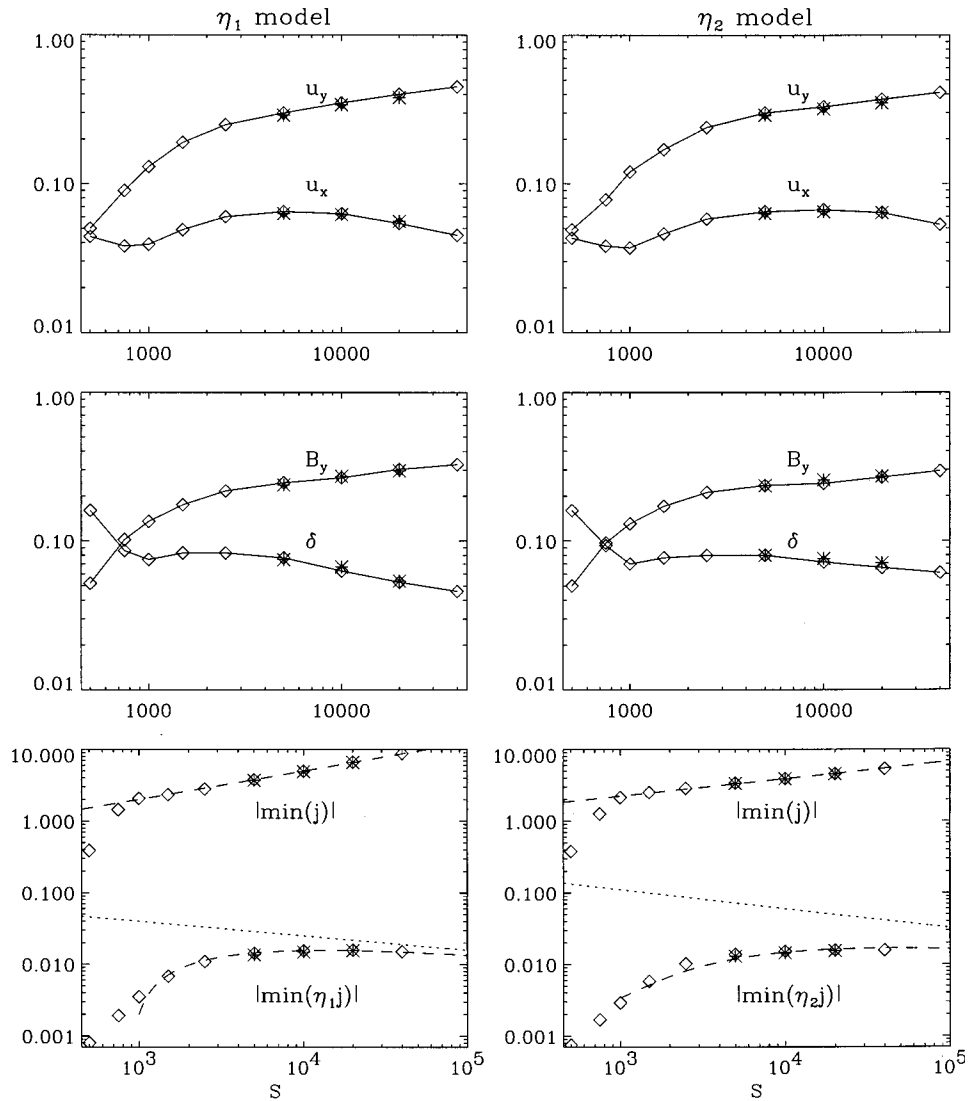


FIG. 7. Scaling of several key parameters in the current sheet between the coalescing islands at $t=t_{\min}$ for the linear η_{an} model (left panels) and the quadratic η_{an} model (right panels); δ —half-width; B_y —maximum field; u_x, u_y —inflow and outflow velocities. The dashed lines show the fits (12), (14) and (21), (23), and the dotted lines are the corresponding asymptotic scalings of the reconnection rate, $R_1^i \sim S^{-0.2}$ and $R_2^i \sim S^{-0.28}$. The meaning of symbols is equal to Fig. 6.

not the rates characteristic of the instability as a whole. Therefore, the reversals of the bulk flow during the resistive phase are of no concern for the scalings obtained here. The values are plotted in Fig. 7. While considering reconnection at the inner current sheet, we have to distinguish between current layer formation without anomalous resistivity ($S \leq 750$) and with anomalous resistivity ($S \geq 1000$). The current sheet length Δ is determined by the width of the coalescing islands and is independent of S in our simulations, as is typical of the coalescence instability. However, as expected, the current sheet half-width δ , the maximum magnetic field B_y , and the current density minimum $j(L_x/2, 0)$ scale in a manner different from simulations with constant resistivity,

$$\delta \sim S^{-0.25}; \quad S \geq 5000, \quad (10)$$

$$B_y \sim S^{0.14}; \quad S \geq 5000, \quad (11)$$

$$j = -0.13S^{0.4}; \quad S \geq 1000, \quad (12)$$

$$u_y \sim S^{0.19}; \quad S \geq 5000. \quad (13)$$

Equations (5) and (12) yield the reconnection rate R_1^i :

$$R_1^i = 0.17S^{-0.2} - 2.5S^{-0.6}. \quad (14)$$

The peak current density minima show nearly the same scaling behavior as the current density maxima at the outer X point for $S \geq 1000$, i.e., in the range where anomalous resistivity occurs. Consequently, the ‘‘inner’’ reconnection rate R_1^i varies in a manner similar to the ‘‘outer’’ reconnection rate R_1^o , i.e., asymptotically it is also ‘‘fast,’’ but no longer ‘‘ultrafast’’ ($\sim S^0$) as in BW and RC.

With the scaling laws for δ , j , and R^i , the upper bound $\bar{\epsilon}_{m, \text{CS}}$ of the Ohmic heating rate in the current sheet, $\epsilon_{m, \text{CS}} = \int_{\text{CS}} \eta j^2 dF$, is determined as

$$\bar{\epsilon}_{m,CS} = 2jR^i \delta \Delta \sim S^{-0.05}. \quad (15)$$

The Ohmic heating is thus expected to decrease only very slowly for large $S (\gg 10^4)$. In comparison, an increase, $\bar{\epsilon}_{m,CS} \sim S^{1/3}$, was found in simulations with constant resistivity.^{3,5} At the same level of approximation, using linear profiles of $B_{x,y}$ and $u_{x,y}$ in the inner current sheet, the local kinetic energy conversion rate $W_{L,CS} = \int_{CS} \mathbf{u} \cdot (\mathbf{j} \times \mathbf{B}) dF$ is obtained as $W_{L,CS} \approx (2/3)j \delta \Delta (u_y B_x + u_x B_y)$, where $j \approx B_y / \delta$ and the maximum values of the variables at the edges of the inner current sheet have been used. Using the numerically obtained scalings for \mathbf{B} and \mathbf{u} at $S \geq 5000$ (cf. Fig. 7), the term $u_y B_x$ is seen to dominate for large S , and the ratio of the local energy conversion rates is found to increase with S like

$$\frac{W_{L,CS}}{\bar{\epsilon}_{m,CS}} \approx \frac{u_y B_x}{3R^i} \sim S^{0.39}. \quad (16)$$

2. Quadratic anomalous resistivity model

A similar analysis of the scaling behavior is done for the η_2 model. Again, a power law gives an excellent fit to the maximum current density at the outer X point (Fig. 6):

$$j = 0.64S^{0.22}. \quad (17)$$

With the quadratic resistivity model, the current density overshoots over j_{cr} at large S and, equivalently, the scaling exponent of j remain somewhat smaller. With (17) and (6) the outer reconnection rate is obtained as

$$R_2^o = 2.6S^{-0.34} - 16S^{-0.56} + 26S^{-0.78}, \quad (18)$$

which is very similar to Eq. (9) over the range of Lundquist numbers used (Fig. 6). At the inner current sheet the following fits are obtained:

$$\delta \sim S^{-0.13}; \quad S \geq 5000, \quad (19)$$

$$B_y \sim S^{0.11}; \quad S \geq 5000, \quad (20)$$

$$j = -0.41S^{0.24}; \quad S \geq 1000, \quad (21)$$

$$u_y \sim S^{0.15}; \quad S \geq 5000, \quad (22)$$

and with (21) and (6) the inner reconnection rate becomes

$$R_2^i = 0.69S^{-0.28} - 6.7S^{-0.52} + 17S^{-0.76}. \quad (23)$$

Again, this is similar to the result for the linear resistivity model (see Fig. 7). The upper bound of the Ohmic heating rate in the inner current sheet scales for large S as

$$\bar{\epsilon}_{m,CS} \sim S^{-0.17}, \quad (24)$$

which decreases more rapidly than in the linear resistivity case due to the smaller current density overshoots. However, the scaling of the local ratio,

$$\frac{W_{L,CS}}{\bar{\epsilon}_{m,CS}} \sim S^{0.43}, \quad (25)$$

at large S turns out to be nearly identical to the linear resistivity case.

3. Discussion

The obtained reconnection rates are nearly independent of the choice of the anomalous resistivity model. Thus, the reconnection rate is the basic parameter of the inner current layer during the coalescence instability. Other parameters like the current density pileup and the Ohmic heating rate adjust themselves according to the reconnection rate and the resistivity model. We attribute small differences in the asymptotic scaling laws of the reconnection rates mainly to their sensitive dependence on the scaling index of j , particularly for the quadratic resistivity model (where the j exponent enters the exponent of R with a factor 3).

The reconnection in the inner current layer is driven by the attraction of the coalescing islands, which does not depend on the Lundquist number in the ‘‘ideal’’ phase. Since the current density and the resistivity can rise freely in the current layer, the rate of reconnection may be expected to be independent of the Lundquist number. Indeed, our data points for the reconnection rate in Fig. 7 are consistent with this conjecture at $S \geq 5000$. (The scaling $R \sim S^0$ was also obtained by BW and RC.) However, the quality of the obtained power law fits to the current density at the coalescence point suggests that the reconnection rate in fact decreases for $S > 10^5$. This may be due to the increasing flux pileup at the current layer for increasing S , which resists the coalescence-driven inflow, or due to a limitation of the current density pileup by the Ohmic heating. The latter effect should be stronger for the linear resistivity model, which shows higher current density pileups. But the reconnection rate is nearly identical (or even slightly higher) with this model, which rules out an important influence of Ohmic heating. The pileup of B_y , on the other hand, increases over the whole range of Lundquist numbers used, its scaling does not strongly depend on the resistivity model, and values $B_y \approx 0.3$ are reached. Although the magnetic pressure still remains an order of magnitude below the external magnetic pressure ($B_0^2 = 1$) in the considered range of S , the repelling force ∇B_y^2 appears to be the dominant factor that limits the reconnection rate (as discussed by BW) and may explain an asymptotic decrease. This argument is further supported by the nearly similar variation of the inflow velocity u_x and the reconnection rate R^i with the Lundquist number (for $S \geq 1000$, where anomalous resistivity is excited; see Fig. 7). Hence, the decrease of the reconnection rate, which was expected by BW to occur at $B_y \sim 0.75B_0$ in a relatively narrow range of Lundquist numbers, appears to take place over a broad range of Lundquist numbers when anomalous resistivity is included. At sufficiently large S values, $B_y \sim 0.75B_0$ will be reached and the reconnection rate will drop further below the values given by (14) and (23) to a scaling $R \sim S^{-1/2}$. With the small scaling exponents for B_y obtained in (11) and (20), this region is not sharply determined but lies at $S > 10^7$ for both resistivity models used in this paper.

The weaker decrease of the current layer half-width δ with S in comparison to its scaling for constant resistivity (where $\delta \sim S^{-2/3}$) is the consequence of a resistivity that rises with j . The outflow velocity u_y is of the order of the Alfvén velocity taken at the point of maximum flux pileup in the inflow region, in agreement with BW. It rises slowly with S ,

different from the RC result, which is due to the driving from the outer X point in our system (cf. the last column in Table I).

The obtained scalings are practically insensitive against the variation of beta. We have found nearly constant reconnection rate R_1^i , current density minimum, and outflow maximum u_y for beta values in the range 10^{-3} –1 and $S = 1000$ (although the compression ratio ρ_{\max}/ρ_{\min} varies from 3.8 for $\beta = 10^{-3}$ to 1.3 for $\beta = 1$ at $t = t_{\min}$).

Figure 7 shows that $\delta \ll l_{CS}(t=0) = (4/\pi)l_{cr}(t=0) = 1$. Therefore, the estimates of the magnitude of the Hall and pressure terms at the onset of kinetic instability given in the Introduction do not necessarily apply to the central current layer during maximum pileup ($t = t_{\min}$). Numerical evaluation of these terms along the inflow and outflow directions at the central current layer shows, however, that both terms remain smaller than the convective term for sufficiently small β ($\leq 10^{-3}$). An exception is the immediate vicinity of the X point, where $u \rightarrow 0$ and $j \neq 0$. Sufficiently close to the X point, the electron fluid and the ion fluid always decouple and collisionless effects become important. We have seen, however, that the inclusion of anomalous resistivity in a low- β plasma leads to diffusive layer widths larger than the scales at which the Hall and pressure gradient terms are non-negligible.

Since the current layer half-width δ approaches small values and since the validity range of our scaling laws for the reconnection rate depends sensitively on the scaling exponent of B_y , it is necessary to guarantee that numerical diffusion does not significantly influence the exponents. This is attempted in our numerical scheme by carefully choosing both the time step and the amount of smoothing required for numerical stability.¹⁵ Moreover, comparison runs with reduced grid spacing gave practically identical results (Figs. 6, 7).

IV. SUMMARY

In this paper we have investigated the coalescence instability in a current sheet with an antiparallel external field in which anomalous resistivity is permitted to occur. The current sheet was initially perturbed by anomalous resistivity spots with nonuniform amplitudes. This form of the coalescence instability is expected to occur in extended current sheets at high Lundquist numbers and low plasma beta. The main results can be summarized as follows.

(1) The dynamic development of the coalescence instability can be divided into two phases. The first, ideal, phase is the approach of the islands with a constant velocity independent of S . The second, resistive, phase is the completion of the coalescence due to magnetic reconnection. This phase is accompanied by plasma jets emanating from the active outer X point and relaxation oscillations of the coalesced island structure. The inclusion of anomalous resistivity into the dynamics does not change the qualitative behavior of the magnetic field and the velocity field during the coalescence process in comparison to simulations with constant resistivity.

(2) A rapid and efficient conversion of magnetic energy

into kinetic energy takes place during the coalescence. By considering time-averaged conversion rates, we have shown that the main part of the energy goes directly into the plasma flow. The main kinetic energy rise occurs within only a few Alfvén transit times (based on the initial O-point separation). Strong maxima of the enstrophy are associated with the vortex flow pattern in the first and second phases of the coalescence.

(3) The scaling behavior of the key quantities in the current layer between the coalescing islands differs from that in simulations with constant resistivity. The flux pileup shows a smaller power law exponent. The peak reconnection rate between the coalescing islands remains nearly constant in the range of Lundquist numbers $S \approx 5 \times 10^3 - 5 \times 10^4$ but is expected to decrease slowly at $S \gg 10^4$, where its scaling is given by $R \sim S^{-\alpha}$ with α in the range $\frac{1}{5} - \frac{1}{3}$, being faster than in the constant resistivity case. In these scalings, S is based on the background resistivity. Following the arguments of Biskamp and Welter³ regarding the scaling of B_y with respect to S , a decrease of the reconnection rate to slow reconnection is expected at $S \geq 10^7$. Nearly identical behavior of the reconnection rate was found for two different models of the anomalous resistivity. For small values of the plasma beta ($\leq 10^{-3}$), the width of the resistive layer exceeds the scales at which the Hall and pressure gradient terms become important. Nevertheless, consideration of the Hall term is necessary in future work, even if anomalous resistivity occurs, to describe the fluid dynamics in the vicinity of the X point correctly.

ACKNOWLEDGMENTS

We gratefully acknowledge helpful comments and criticism by F. Jamitzky, M. Scholer, and an anonymous referee.

This work was supported by Grants No. 50QL9208 and 50QL9301 of the Deutsche Agentur für Raumfahrtangelegenheiten.

¹J. M. Finn and P. K. Kaw, Phys. Fluids **20**, 72 (1977).

²P. L. Prichett and C. C. Wu, Phys. Fluids **22**, 2140 (1979).

³D. Biskamp and H. Welter, Phys. Rev. Lett. **44**, 1069 (1980).

⁴A. Bhattacharjee, F. Brunel, and T. Tajima, Phys. Fluids **26**, 3332 (1983).

⁵G. J. Rickard and I. J. D. Craig, Phys. Fluids B **5**, 956 (1993).

⁶T. Tajima, F. Brunel, and J. Sakai, Astrophys. J. Lett. **258**, L45 (1982); T. Tajima, J. Sakai, H. Nakajima, T. Kosugi, F. Brunel, and M. R. Kundu, Astrophys. J. **321**, 1031 (1987).

⁷M. Scholer, Geophys. Monograph **58**, 85 (1990).

⁸J. N. Leboeuf, T. Tajima, and J. M. Dawson, Phys. Fluids **25**, 784 (1982).

⁹W. H. Matthaeus and S. L. Lamkin, Phys. Fluids **29**, 2513 (1986).

¹⁰V. M. Fadeev, I. F. Kvaratskhava, and N. N. Komarov, Nucl. Fusion **5**, 202 (1965).

¹¹See AIP Document No. PAPS PHPAE-03-4703-16 for 16 pages of Report No. PPG-511, "Magnetic islands coalescence and intense plasma heating," by C. C. Wu, J. N. Leboeuf, T. Tajima, and J. M. Dawson, 1980. Order by PAPS number and journal reference from the American Institute of Physics, Physics Auxiliary Publication Service, Carolyn Gehlbach, 500 Sunnyside Blvd., Woodbury, NY 11797-2999. Fax: 516-576-2223; electronic mail: paps@aip.org. The price is \$1.50 for each microfiche (98 pages) or \$5.00 for photocopies of up to 30 pages, and \$0.15 for each additional page over 30 pages. Airmail additional. Make checks payable to the American Institute of Physics.

¹²S. V. Bulanov, S. I. Syrovatsky, and J. Sakai, JETP Lett. **28**, 177 (1978).

¹³X. Wang and A. Bhattacharjee, Astrophys. J. **420**, 415 (1994).

¹⁴P. A. Isenberg, T. G. Forbes, and P. Démoulin, Astrophys. J. **417**, 368 (1993).

- ¹⁵J. Schumacher and B. Kliem, *Phys. Plasmas* **3**, 4703 (1996).
- ¹⁶R. L. Richard, R. J. Walker, R. D. Sydora, and M. Ashour-Abdalla, *J. Geophys. Res.* **94**, 2471 (1989).
- ¹⁷K. Papadopoulos, in *Dynamics of the Magnetosphere*, edited by S. I. Aka-sofu (Reidel, Dordrecht, 1979), p. 289.
- ¹⁸J. D. Huba, N. T. Gladd, and K. Papadopoulos, *J. Geophys. Res.* **83**, 5217 (1978).
- ¹⁹J. D. Huba, N. T. Gladd, and J. F. Drake, *J. Geophys. Res.* **86**, 5881 (1981).
- ²⁰P. H. Yoon, A. T. Y. Lui, and C.-L. Chang, *Phys. Plasmas* **1**, 3033 (1994).
- ²¹R. C. Davidson, N. T. Gladd, C. S. Wu, and J. D. Huba, *Phys. Fluids* **20**, 301 (1977).
- ²²R. C. Davidson, N. T. Gladd, and Y. Goren, *Phys. Fluids* **21**, 992 (1978); J. D. Huba, N. T. Gladd, and J. F. Drake, *J. Geophys. Res.* **87**, 1697 (1982).
- ²³K. Papadopoulos, *Rev. Geophys. Space Phys.* **15**, 113 (1977).
- ²⁴G. Benford, *Astrophys. J.* **269**, 690 (1983).
- ²⁵J. F. Drake, R. G. Kleva, and M. E. Mandt, *Phys. Rev. Lett.* **73**, 1251 (1994).
- ²⁶D. Biskamp, E. Schwarz, and J. F. Drake, *Phys. Rev. Lett.* **75**, 3850 (1995); D. Biskamp, E. Schwarz, and J. F. Drake, *Phys. Plasmas* **4**, 1002 (1997).
- ²⁷M. Ugai and T. Tsuda, *J. Plasma Phys.* **17**, 337 (1977); M. Ugai, *Plasma Phys. Controlled Fusion* **26**, 1549 (1984).
- ²⁸E. R. Priest and T. G. Forbes, *J. Geophys. Res.* **91**, 5579 (1986).